NANOSYSTEMS: PHYSICS, CHEMISTRY, MATHEMATICS, 2013, 4 (2), P. 276–287

PARTICIPATION OF NANOCRYSTALLINE TiO_2 SURFACE IN THE ELECTRON TRANSFER BETWEEN SEMICONDUCTOR SOLID AND ADSORBED COBALT(III)-*R*PY COMPLEX

A. S. Ganeshraja[1], K. Anbalagan[1]

[1] Department of Chemistry, Pondicherry University Kalapet, Pondicherry 605 014, India
asgchem84@gmail.com, kanuniv@gmail.com

PACS 81.20.-n, 61.72.uj

Cis-$[Co^{III}(tn)_2(R\text{py})Br]Br_2$, ($R$ = 4-CN, H, *4*-Bz, *4*-Me, *4*-Et, and *4*-MeNH), in aqueous 2-propanol exhibit varying adsorption characteristics and led to surface compound formation. UV (λ = 254) excitation of the nano-TiO_2//cobalt(III)-(Rpy) surface compound resulted in interfacial electron transfer (IFET) reaction. The IFET has been found to be dependent upon the coordination environment of the complex, more precisely due to the Rpy ligand. In addition, the proposed mechanism of the IFET reaction includes the formation of a Co^{II} ion implanted in nanocrystalline TiO_2. This photoreduction was found to be solvent controlled. The photoefficiency of the Co^{II}_{aq} formation was spectrally analyzed simultaneously as Co^{II}:TiO_2 was isolated from the photolyte solution. The isolated solid was subjected to FTIR, DRS, PXRD, and SEM-EDX instrumental analysis. It is concluded that the removal of metal ion in the form of a complex is coordination structure dependent, hence, seems more specific in removal efficiency and in doping the anatase lattice.

Keywords: surface adsorption, interfacial electron transfer reaction, cobalt doped nano-TiO_2.

1. Introduction

Interfacial electron transfer (IFET) between sensitizer molecular adsorbates and semiconductor materials has been a subject of intense research in recent years. Examples include, among others, photocatalysis [1], surface photochemistry [2,3], dye-sensitized solar cells (DSSCs) [4], organic semiconductor-based photovoltaics [5], and nanoscale optoelectronics based on a single molecule or a small group of molecules [6]. This is a fundamental process in surface chemistry, relevant to a broad range of practical applications, including effective mechanisms of solar energy conversion [7,8], photoelectrochemistry [9], artificial photosynthesis and imaging [10]. Despite its great technological significance, IFET remains poorly understood [1,2] compared to electron transfer in homogeneous solutions [11].

At present, TiO_2 is considered as the most promising photocatalyst because of its low cost, nontoxicity, excellent stability, and high efficiency [12]. However, it can be activated only through irradiation with ultraviolet (UV) light (4–5 % of solar light) because of its large band gap of 3.0 eV to 3.2 eV [13]. Thus, many attempts have been made to enhance the photocatalytic activity of TiO_2 in the visible light range. Doping with transition metals (Cr, Co, V, Fe, etc.) is one of the promising approaches [14]. Co(II) is considered as one of the more promising candidates because of its effect in reducing the electron–hole recombination rate and in shifting the absorption edge into the visible light region. Co-doped TiO_2 has shown high activities for degradation of acetaldehyde, 2-chlorophenol, and 2,4- dichlorophenol in aqueous solutions [15]. Transition metal-doped

TiO_2 photocatalysts are active under visible light irradiation. However, these materials have certain disadvantages, such as thermal instability as well as low quantum efficiency of the photoinduced charge carriers [16,17]. To overcome these drawbacks, considerable effort has been exerted to modify the properties of transition metal-doped TiO_2 using nonmetal impurities [18]. In this work, the luminescence properties of anatase TiO_2 samples doped with different amounts of Co^{2+} when were excited using a source with energy (2.54 eV), well below the TiO_2 bandgap, is reported. The effect of introducing defects through the incorporation of Co atoms in the TiO_2 lattice is discussed. With this approach the electron–hole recombination, which is excitonic in nature, is not excited because laser energies greater or on the order of the bandgap are required; instead, this study is focused on the defects-related emission band observed by Sekiya et al. [19] at 1.95eV (77 K). In our sol–gel samples, this band was observed at 2.02eV at room temperature [20].

Understanding the photophysics of transition metal complexes attached to semiconductor surfaces is essential for the design of artificial systems for solar energy conversion. In particular, Cobalt(III)-pyridyl complexes have attracted a great deal of attention as a promising class of compounds with long-lived charge-separated states and rich photochemical properties. However, their electronic excitations and photoconversion mechanisms remain only partially understood. This paper builds upon our recent work [21,22] and addresses the study of TiO_2 nanoparticles sensitized with *cis*-$[Co^{III}(tn)_2(R\text{py})Br]Br_2$ (where *R*=*4*-CN, H, *4*-Bz, *4*-Me, *4*-Et, and *4*-MeNH) adsorbates. Our study includes the characterization of the electronic excitations, electron injection time scales, and IFET mechanisms [23] IFET photoefficiency and photo degradation of 2-propanol. Here, we focus on TiO_2 surfaces modified by Co(III)-pyridyl complexes attached by nitrogen linkers. Emphasis is given to the characterization of the electronic excitations and injection time scales as determined by the nature of the molecular adsorbates and the attachment modes.

2. Experimental

2.1. Materials and methods

$CoCl_2.6H_2O$ (99%), *R*-pyridine (*R*py), ferric chloride, potassium oxalate, sodium acetate, ammonium thiocyanate, nanocrystalline titanium dioxide (surface area = 200–220 m^2/g and particle size = 25 nm) and DMSO-d_6 (NMR solvent) were purchased from Sigma Aldrich. 1,3-diamino propane (LR), pyridine, 1,10-phenanthroline and all other chemicals were purchased from Himedia and SD. Fine Chemicals (India). All the solvents and 1,3-diamino propane were purified by distillation and water was triply distilled over alkaline $KMnO_4$ in an all glass apparatus. Analytically pure crystals of *cis*-$[Co^{III}(tn)_2(R\text{py})Br]Br_2$ adsorbates (where *R* = *4*-CN, H, *4*-Bz, *4*-Me, *4*-Et, and *4*-MeNH) were synthesized by a modified procedure [24] and recrystallized.

2.2. Instrumentation

Cobalt(III) complexes were photolysed using a 254 nm, 6 watt low pressure mercury vapor lamp as the light source (Germicidal G4T5, 3H, model 3006) in a small quartz immersion well (model 3210, 80 mL cap. Photochemical Reactors Ltd, UK). Electronic absorption spectral studies were undertaken on a double beam spectrophotometer (Shimadzu 2450, Japan) with integrating sphere attachment (ISR-2200). UV-vis diffuse reflectance spectra (UV-vis DRS) were recorded in absorbance mode at room temperature in the 200–1000 nm range on a Shimadzu, (UV 2450) double-beam spectrophotometer equipped

with integrating sphere attachment (ISR-2200) using $BaSO_4$ as the reference. The instrument is interfaced with a computer for data collection and analysis. Fourier transform infrared (FTIR) spectra were recorded in the 4000–400 cm^{-1} range using a Thermo Nicolet 6700 FTIR spectrophotometer using KBr wafer with resolution 0.1 cm^{-1}. ^1H NMR measurements were made on a Bruker instrument; model Avance-II in 400 MHz Fourier transform-nuclear magnetic resonance with DMSO-d_6 solvent. PXRDs were collected on an 800 W Philips (PANANALYTICAL, Almelo, The Netherlands) powder diffractometer equipped with an etched glass plate sample holder by rotating anode diffractometer in the 2θ range 10–80 ° with step size of 0.02 ° using Cu Kα (λ = 1.5406 Å) radiation to determine the identity of any phase and their crystalline size. Surface morphology and chemical mapping were examined by SEM (Hitachi, S-3400N microscope), operating at 0.3-30 kV. Microanalyses (energy dispersive X-ray analysis, EDX) were performed with Thermo SuperDry II attachment of SEM.

2.3. Photocatalytic activity measurement

The photocatalytic activity of nano-TiO_2 was evaluated by measuring the efficiency of the reduction of the $Co^{III}(tn)_2(R\text{py})Br^{2+}$ complex in neat water/aqueous 2-propanol solutions under 254 nm light irradiation. The photoefficiency was calculated by estimating photogenerated Co^{II} by Kitson's method [25]. Photoreduction was carried out in a reactor vessel using a 254 nm low pressure mercury vapor lamp, which were housed in a fume hood (Lab Guard), covered with black polythene sheet to prevent extraneous light. The photoreactor is a double walled quartz vessel, in which, photolyte mixture (100 mg of nano-TiO_2 crystals in 80 mL of *cis*-$Co^{III}(tn)_2(R\text{py})Br^{2+}$ (1.68×10^{-3} M) solution and 1M $NaNO_3$) was taken in the inner jacket and cool water in the outer jacket. Prior to irradiation, the suspension of the catalyst was achieved by ultrasonic treatment and continued magnetic stirring in the dark to attain cobalt(III) complex ion adsorption/desorption equilibrium on the catalyst. The photolyte suspension was irradiated with 254 nm light for defined periods (0, 2–16 min). About 4 mL aliquots were sampled and centrifuged to remove the semiconductor particles and then spectrally analyzed. In order to diminish experimental error, experiments were repeated at least two-three times for the same sample and the mean value was calculated. Photoefficiency of Co(II) formation in terms of percentage, PE (%) was computed using the formula: PE (%) = $[(A_t - A_i)/A_t] \times 100$ where A_i and A_t are the absorbances of the photolysed solutions initially and at definite time interval 't' respectively.

3. Results and discussion

3.1. Photocatalytic reduction of $Co^{III}(tn)_2(R\text{py})Br^{2+}$

Cobalt(III)-*R*pycomplex is a good UV light absorber, however, it decomposes on exposure to light over a long period of time due to ligand to metal charge transfer (LMCT) bands (λ =~356 nm). Surprisingly, the addition of nano-TiO_2 (anatase) provoked the complex to degrade more efficiently and a higher amount of cobalt(II) was generated. Figure 1 depicts repetitive scan spectra of $Co^{III}(tn)_2$(4-Etpy)Br^{2+} complex observed at defined irradiation time intervals; there is a blue shift in the absorption maxima at λ = 357 → 351 nm and red shift at λ = 512 → 518 nm. The absence of an isosbestic point in the repetitive scan spectra indicates the decomposition of the complex during the reduction process suggesting, perturbation of the Co^{III} centre due to IFET. The photoefficiency of Co(II) formation by TiO_2 (e^-_{cb}/h^+_{vb})/scavenger of $Co^{III}(tn)_2$(4-Etpy)Br^{2+} is increased with respect

to the concentration of 2-propanol and more active at higher concentrations in the photolytic solutions. This implies the observed photoefficiency (Table 1) for the formation of Co^{II} is a summation of the individual electron transfer reactions due to (i) excited nano-TiO_2: $Co^{III}(tn)_2(R\text{py})Br^{2+}$ + nano-TiO_2 + hν (λ = 254 nm) $\rightarrow$ Co^{II} + products and (ii) ligand to metal charge transfer transition in cobalt(III) complex: $Co^{III}(tn)_2(R\text{py})Br^{2+}$ + hν (λ = 254 nm) $\rightarrow$ Co^{II} + products. However, the former path is predominant and requires a thorough investigation.

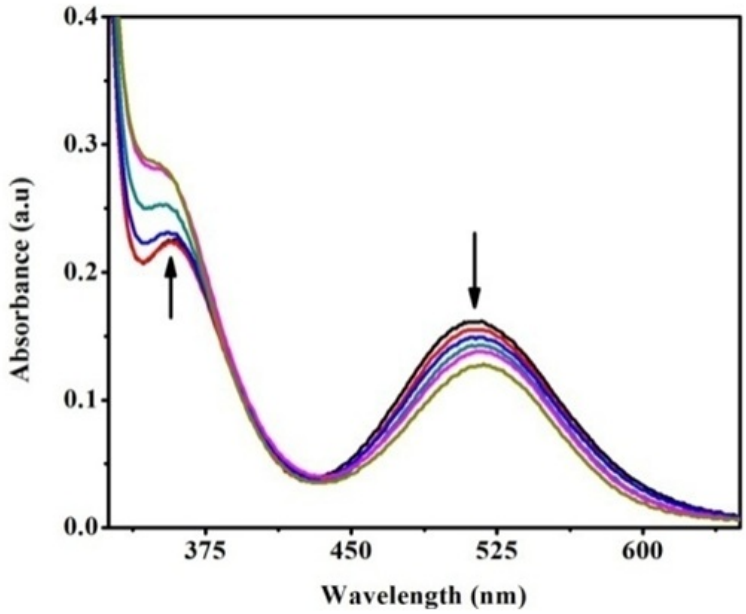

Fig. 1. Repetitive scan spectra recorded for the photocatalysed $Co^{III}(tn)_2$ (4-Etpy)Br^{2+} complex ion in nano-TiO_2 suspension in neat water at various time intervals: 0, 2, 4, 8, 12 and 16 min respectively. Complex concentration = 1.68×10^{-3} *M*, ionic strength = 1*M* $NaNO_3$, pH $\sim$ 7 and at 298 K

In the case of photoreduction of $Co^{III}(tn)_2(R\text{py})Br^{2+}$ complex with nanocrystalline titania influence than that of polycrystalline titania. Nanocrystalline materials are single- or multi-phase polycrystalline solids with a grain size of a few nanometers (1 nm = 10^{-9} m = 10 Å), typically less than 100 nm. Since the grain sizes are so small, a significant volume of the microstructure in nanocrystalline materials is composed of interfaces, mainly grain boundaries, i.e., a large volume fraction of the atoms resides in grain boundaries. Consequently, nanocrystalline materials exhibit properties that are significantly different from and often improved over, their conventional coarse-grained polycrystalline counterparts [26]. In polycrystalline wide band gap oxide semiconductors such as ZnO and TiO_2, the photoconductivity (PC) has been observed to decay very slowly, over a period of many hours to several days [27,28]. This slow decay is often referred to as 'persistent PC' and different possible explanations have been proposed [29-31]. In some cases, models have been fitted to the experimental data for the determination of electronic parameters of the materials, such as the energy distribution of charge carrier traps [32,33] Photocatalytic degradation studies of pollutants using either Co(II)-tetrasulfophthalocyanine grafted on TiO_2 via a silane reagent or polycrystalline TiO_2 samples impregnated with Cu(II)-phthalocyanine [32] were reported in the literature.

Table 1. Photoefficiency P.E (%) of formation of Co(II) upon λ = 254 nm irradiation of *cis* $Co^{III}(tn)_2(Rpy)Br^{2+}$ in aqueous 2-propanol at 298 K. ionic strength 1*M* $NaNO_3$, complex concentration = 1.68×10^{-3}*M*

*R*py	PE (%) in water/Pr^{i}OH(w/w)%							pKa value of *R*py
		100/0	95/5	90/10	85/15	80/20	75/25	70/30	
4-CN	-	14±0.5	18±1.0	19±1.0	21±0.7	26±0.8	28±0.9	32±0.6	1.90
	poly-TiO_2	16±1.0	17±0.5	21±1.0	24±0.8	29±0.7	31±0.6	37±0.5	
	nano-TiO_2	17±0.7	20±0.9	24±0.5	29±0.8	31±0.6	37±1.0	41±1.4	
H	-	15±0.8	21±0.7	29±1.0	34±0.5	38±1.4	40±0.9	42±1.2	5.25
	poly-TiO_2	14±0.6	24±1.0	32±0.8	35±0.8	41±0.7	44±0.9	48±1.2	
	nano-TiO_2	18±1.0	25±0.7	34±0.6	39±1.0	45±0.5	51±0.9	55±0.5	
4-Bz	-	12±0.8	19±1.0	24±0.6	28±0.7	32±0.8	38±0.5	41±1.2	5.59
	poly-TiO_2	16±0.6	23±0.8	28±1.0	30±1.4	34±0.5	38±0.9	49±0.8	
	nano-TiO_2	18±0.6	21±0.8	29±0.7	31±0.5	36±1.0	44±0.9	57±1.4	
4-Me	-	12±1.0	19±1.0	26±0.5	29±0.8	34±0.9	38±0.8	49±1.4	6.02
	poly-TiO_2	17±1.0	23±0.5	29±0.6	34±0.8	37±0.9	45±0.9	52±0.7	
	nano-TiO_2	19±0.7	26±0.5	33±1.0	38±0.6	46±0.8	54±1.4	57±0.9	
4-Et	-	18±1.2	24±0.6	28±1.0	31±0.5	36±1.4	41±0.8	49±0.5	6.02
	poly-TiO_2	19±1.0	27±1.0	32±0.9	37±0.8	45±0.5	48±0.8	53±1.4	
	nano-TiO_2	21±0.6	28±0.5	35±1.0	39±0.9	49±0.8	58±0.5	64±0.7	
4-MeNH	-	19±0.8	24±0.5	29±0.5	32±1.0	46±1.0	52±0.8	53±0.9	9.70
	poly-TiO_2	23±0.7	28±0.8	32±0.5	38±0.6	49±1.0	58±0.9	61±0.5	
	nano-TiO_2	26±0.8	31±0.6	37±0.7	44±0.5	54±1.0	63±0.9	69±0.8	

3.2. Photo-oxidation of 2-propanol to acetone by ^{1}H NMR

The photoreduction was systematically followed by NMR measurements which indicate the growth of acetone peak progressively appearing in signal intensity as a function of dosage of light [34]. Table 2 exhibits ^{1}H NMR signals due to 2-propanol appearing at δ = 1.0 to 1.1 ppm (-CH_3) and δ = 3.8 to 3.93 ppm (-CH) before the initiation of photoreduction and after defined irradiation periods. There is a steady growth of the signal due to photo released acetone and the signal intensity increases with respect to the level of light irradiation. That is, a new ^{1}H NMR signal at δ = 2.04 ppm indicates the formation of acetone and the signal strength (Table 2) increases considerably with increased irradiation times [35]. In fact, the integrated intensity of the acetone signals gradually increase, whereas the -CH and -CH_3 (2-propanol) signals gradually decrease. The origination of acetone is from the oxidation of 2-propanol resulting from the scavengingof valence band holes by the alcohol: nano-TiO_2 (h^+) + $(CH_3)_2CHOH \rightarrow CH_3COCH_3$.

3.3. Mechanism of photoinduced electron transfer reaction

It is apparent from Table 1 that excited nanocrystalline TiO_2 shows better catalytic activity, which critically depends upon the surface-substrate interaction. Surface affinity of molecules/ions is a competing feature of the surface, therefore, formation of poly (or) nano-TiO_2//cobalt(III)-(*R*py) surface compound is inevitable. Therefore, an enhancement

Table 2. ^{1}H NMR data for the generator of acetone upon λ = 254 nm irradiation of $Co^{III}(tn)_2$(4-Etpy)Br^{2+} at 298 K in DMSO-d_6. Photocatalyst nano-TiO_2, ionic strength 1N $NaNO_3$, complex 1.86×10^{-3}M. 'A' and 'P', respectively, denote acetone and 2-propanol

Irradiating time (min)	2x -CH_3(d) P δ ppm		-CH(m) P δ ppm							2x -CH_3(s) A δ ppm
0	0.98	0.99	3.72	3.73	3.75	3.61	3.78	3.79	3.81	-
8	0.98	0.99	3.72	3.73	3.75	3.76	3.78	3.79	3.81	2.02
16	0.98	0.99	3.72	3.73	3.75	3.76	3.78	3.79	3.81	2.02
45	0.98	0.10	3.71	3.73	3.75	3.76	3.77	3.79	3.80	2.02

in the photocatalytic reduction originates from (i) *R*py can modify the surface affinity of $Co^{III}(tn)_2(R\text{py})Br^{2+}$ ion with the nano-TiO_2 surface and (ii) photoexcitation can prompt the formation of microdomains in nano-TiO_2 with characteristic hydrophobic/hydrophilic behavior. Therefore, accumulation of adsorbate is varied, and hence, available for reduction. In addition, charge relaxation/recombination processes of nano-TiO_2 (e^-, h^+) pair are altered due to the formation of compact nano-TiO_2//cobalt(III)-(*R*py) surface compound, (Co^{III}_{ad}). Such processes provide a favorable negative charge potential for reduction of the Co(III) center. Thus, the overall efficiency of heterogeneous photocatalysis is determined by the adsorbate content and population/lifetime of the charge carriers for interfacial charge-transfer processes [36,37]. Sixth ligand (*R*py) in $Co^{III}(tn)_2(R\text{py})Br^{2+}$ with a hydrophobic tail imparts variation in surface adherence of the complex ion on the surface of nano-TiO_2, however, the adsorption process is restricted by thermodynamic aspects. To rationalize these observations, one must invoke a mechanism that incorporates several complementary routes as given in eqs. (1-7).

Surface compound formation: nano-TiO_2 + $Co^{III}(tn)_2(R\text{py})Br^{2+}$ → nano-TiO_2// $Co^{III}(tn)_2(R\text{py})Br^{2+}$ (1)

Photoexcitation: nano-TiO_2 + $h\nu$ → nano-TiO_2(e^-, CB) + nano-TiO_2(h^+, VB) (2)

Charge trapping: (e^-, CB) → (e^-, tr) (3)

(h^+, VB) → (h^+, tr) (4)

Electron-hole recombination: (e^-, tr)/(e^-,CB)+ (h^+,tr)/(h^+, VB)→(e^-,tr)+heat (5)

Electron transfer: nano-TiO_2 (e^-, CB)/ (e^-, tr) + (Co^{III}_{ad}) → Co^{II}_{surf} + Co^{II}_{aq} (6)

Hole transfer: nano-TiO_2(h^+, VB)/ nano-TiO_2 (h^+, tr)+$(CH_3)_2CHOH$→CH_3COCH_3 (7)

Where (e^-, tr) and (h^+, tr) represent charge trapped surface states while Co^{III}_{ad}, Co^{II}_{surf}, and Co^{II}_{aq} represent surface compound, surface implanted species and aqueous species respectively. It is unlikely that the photoreduction of Co(III) proceeds through multielectron process, but it should occur in one electron step. The predominant reduction path of the metal centre is as given in eqs. 1-7 with a limited contribution from charge transfer population states like: σ(N) → dσ*(Co) and σ(Cl) → Co.

3.4. *p*Ka dependent photoreduction

In this investigation, a linear dependence of photoefficiency(%) of $Co^{III}(tn)_2(R\text{py})Br^{2+}/TiO_2$ suspension with respect to the *R*pyligand in terms of acidity constant (*p*Ka)

as shown in Figure 2 is observed. Linear regression analysis of PE% versus pKa yields a slope indicating that electron donating groups in Rpy (pKa > 5.25) enhances photo efficiency (%) and that electron withdrawing groups in Rpy (pKa = 1.90) reduces the photo catalytic behavior. Therefore, it can be concluded that coordination environment of the metal centre of a transition metal ion can greatly influence the photochemical character of the complex.

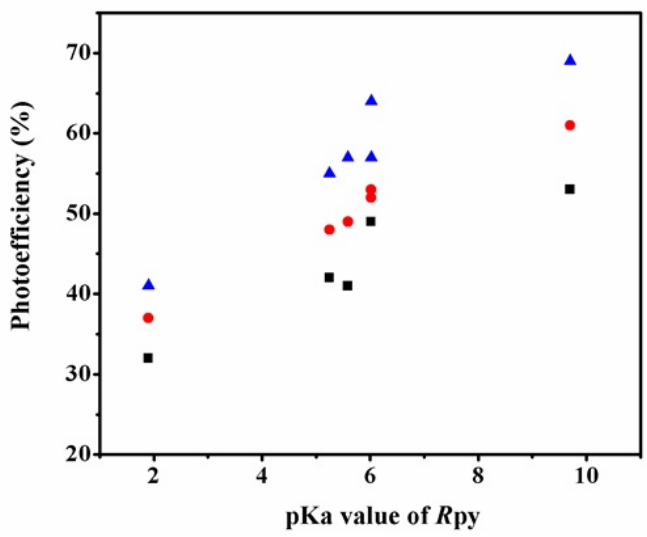

Fig. 2. Linear plot of photoefficiency *vs*. pKa value of aryl amine (R) in $Co^{III}(tn)_2(R\text{py})Br^{2+}$; ■ absence of nano-$TiO_2$, ● presence poly-$TiO_2$, and ▲ presence nano-$TiO_2$ in 70/30 (w/w)% water/Pr^iOH

It is interesting to note that the PE (%) of Co^{II} generation is (i) linearly increasing with 2-propanol content and (ii) showing some relationship with variation in the Rpy ligand of the complex. This non-consistency can be attributed to nanoparticle (or polycrystalline) surface//cobalt(III)-Rpy affinity and subsequent interfacial electron transfer. Accumulation of cobalt(III) complex on the surface of nano-TiO_2 to form a compact layer is mainly dependent upon the blocking effect of Rpy due to electron withdrawing and electron donating properties. Pellizzetti and co-workers showed a significant alteration in the distribution of aromatic intermediates on the surface of TiO_2 in their study [38]. Figure 2 shows photoefficiency *vs* pKa of the aryl amine of the Rpy ligand of six $Co^{III}(tn)_2(R\text{py})Br^{2+}$ complexes. It is interesting that, within this limited set of complexes at least, there is an obvious relationship between PE and the pKa value of the ligand. There is a reasonable enhancement in the PE with aromatic ring electronic nature of the Rpy ligand, which appears to asymptotically approach a limiting value.

3.5. Characterizations of cobalt-doped nano-TiO_2

The isolated solids were subjected to spectral, macrostructural, microstructural, and surface morphological analyses. Therefore, the irradiated $Co^{III}(tn)_2(R\text{py})Br^{2+}$ with nanocrystalline TiO_2 were subjected to FTIR, DRS, PXRD and SEM-EDX analyses. The experimental results yield the characteristic features on the inclusion of cobalt ion in anatase lattice, which was confirmed by XRD patterns. XRD and SEM results revealed that the particle size of Co-doped nano-TiO_2 is enhanced as the result of the UV-light irradiation method. Here, we focus on TiO_2 surfaces modified by $Co^{III}(tn)_2(R\text{py})Br^{2+}$

complexes attached by nitrogen linkers. Emphasis is given to the characterization of the electronic excitations and injection time scales as determined by the nature of the molecular adsorbates and the attachment modes.

3.6. FTIR, DRS and powder X-ray difraction analysis of Co/nano-TiO_2

Transmittance peaks observed between 450–600 cm^{-1} can be assigned to the Ti-O-Ti bond as shown in Figure 3(A). Both pure and Co-doped nano-TiO_2 showed a characteristic band at 511 cm^{-1} corresponding to a Ti-O bond of the anatase phase. Ti-O vibration tends to shift to lower energy regions with Co content in nano-TiO_2. The DRS of undoped anatase [39] showed 100% reflectance, and doped samples absorb more effectively from 480–600 nm. Nano-TiO_2 with low cobalt density absorbs at ~563 nm, and the λ_{max} shifts towards ~574 nm (Figure 3(B)). The red shift is attributed to the 3d Co^{2+} electrons into the conduction band of nano-TiO_2. The absorption spectrum of TiO_2 consists of a single broad intense absorption around 400 nm due to the charge-transfer from the valence band (mainly formed by $2p$ orbitals of the oxide anions) to the conduction band (mainly formed by $3d$ t_2g orbitals of the Ti^{4+} cations) [40]. Pure TiO_2 showed absorbance in the shorter wavelength region while Co/TiO_2 and the DRS results showed a red shift in the absorption onset value in the case of Co-doped titania. The doping of various transition metal ions into TiO_2 could shift its optical absorption edge from the UV into the visible light range, but no prominent change in the TiO_2 band gap was observed [40].

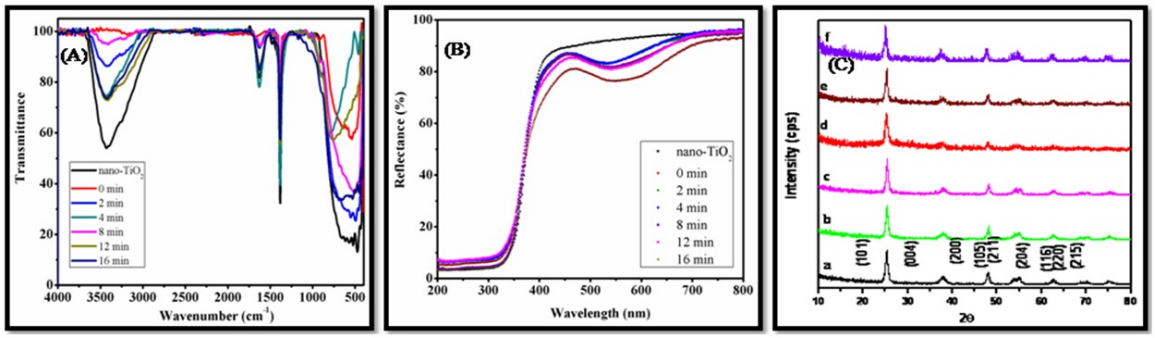

Fig. 3. (A) Diffuse reflectance spectra, (B) FT-IR spectra and (C) PXRD pattern of the pure nano TiO_2 and x%Co:nano-TiO_2

Figure 3(c) shows the X-ray diffraction patterns of the undoped and cobalt-doped TiO_2 samples. The nanocrystalline anatase structure was confirmed by (1 0 1), (0 0 4), (2 0 0), (1 0 5) and (2 1 1) diffraction peaks [41,42]. The XRD patterns of anatase have a main peak at 2θ = 25.2° corresponding to the 101 plane (JCPDS 21-1272) while the main peaks of rutile and brookite phases are at 2θ = 27.4° (110 plane) and 2θ = 30.8° (121 plane), respectively. Therefore, rutile and brookite phases have not been detected [43,44]. The XRD patterns didn't show any Co phase (even for 5% Co/TiO_2 sample) indicating that Co ions were uniformly dispersed among the anatase crystallites. In the region of 2θ = 10–80°, the diffractive peak shapes of pure TiO_2 crystal planes are quite similar to that of Co/TiO_2 with different concentrations of Co. The XRD patterns indicate pure anatase phase [45] form and confirm the absence of phase transformation to other related crystalline phases like rutile and brookite. This indicates that only a small amount of the elements are substituted into the Ti^{4+} sites, while interstitially incorporated Co(II) cannot be discounted as shown in Figure 3(C).

Table 3. The chemical content of cobalt doped TiO_2 samples, recorded for nano-TiO_2/Co,x% prepared by UV sensitized photoreduction of (1.63×10^{-3} M) $Co(tn)_2(4\text{-}Mepy)Br^{2+}$ in water at various time interval of irradiation and at 27 ° according to the Energy Dispersive X-ray analysis

Irradiation Time(min)	Abbreviation of Sample	Content Weight % (atm. %)		
		Ti	O	Co
-	nano-TiO_2	59.95 (33.33)	40.05 (66.67)	-
0	nano-TiO_2/Co,0.26 atm. %	60.05 (33.40)	40.32 (67.12)	0.26(0.12)
2	nano-TiO_2/Co, 0.53 atm. %	51.29 (26.18)	48.17 (73.60)	0.53 (0.22)
4	nano-TiO_2/Co, 0.68 atm. %	35.89 (15.86)	63.43 (83.90)	0.68 (0.25)
12	nano-TiO_2/Co, 0.50 atm. %	30.66 (12.93)	68.85 (86.90)	0.50 (0.17)
16	nano-TiO_2/Co, 0.71 atm. %	36.97 (16.49)	62.32 (83.25)	0.71 (0.26)

3.7. Surface Morphology of cobalt doped nano-TiO_2

The morphology of the undoped TiO_2 sample is shown in Figure 4, revealing that the agglomeration of nanocrystals form particles or grains, which are expected to contribute more grain boundary effects. The chemical compositions of undoped and doped samples are very essential to know the exact concentration of the dopant (Co here) and the defects. The EDAX spectrum of undoped TiO_2 shows the presence of Ti and O elements alone in the sample, confirming the absence of any impurities. The atomic percentage of Ti and O elements in undoped TiO_2 sample is 59.95 and 40.05, respectively, but actual stoichiometric atomic percentage of Ti is 36.97 and O is 62.32, which shows oxygen deficiency in the undoped TiO_2 sample. Likewise, all the doped samples show oxygen deficiency. Table 3 gives the atomic percentage of Ti, O, and Co. SEM images illustrate that the particles, which mainly belong to anatase phase, are loosely agglomerated, spherical and a few hundred nm in size (Figure 4(A)). Homogeneous and continuous surface structure with well dispersed spheres appear as the dopant density in Co/TiO_2 is increased (Figure 4(B)(C)).

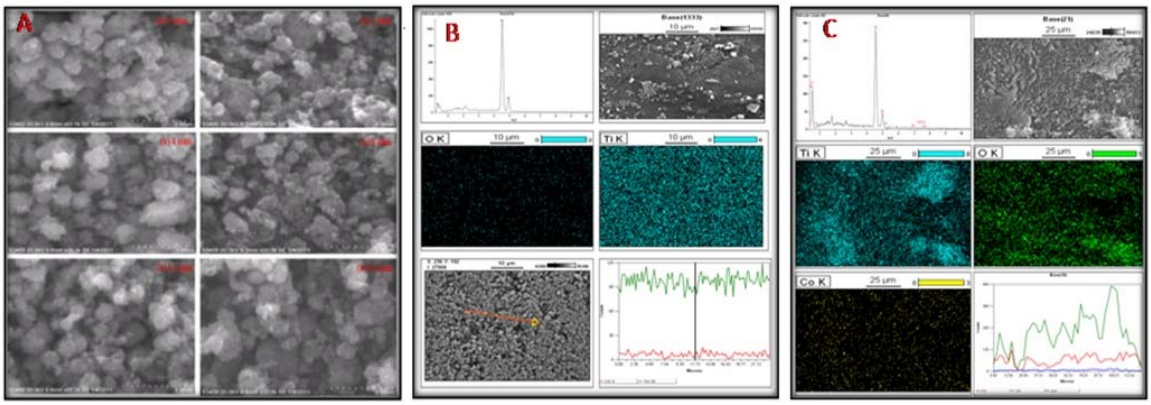

Fig. 4. (A) SEM images and (B), (C) EDX spectra, mapping, line spectra of pure nano-TiO_2 and x%Co:nano-TiO_2 particles

4. Conclusion

We have demonstrated that *cis*-$[Co^{III}(tn)_2(R\text{py})Br]Br_2$ complexes are photocatalytically reduced into Co^{II}_{sol}. The photoreduction is found to be solvent dependent. The photoproduced acetone illustrates the scavenging effect of isopropanol. The IFET reaction mechanism is important to understand the functioning and construction of nano-TiO_2 photocatalysed photochemical energy conversion systems. It is concluded that the removal of metal ion, hence, seems more specific in removal efficiency and in doping the anatase lattice.

Acknowledgment

KA is thankful to the CSIR (sanction order: No. 01(2570)/12/EMR-II/3.4.2012), New Delhi for financial support through major research project. ASG is thankful to Mr. S. Thirumurugan and Mr. Kanniah Rajkumar, Department of Chemistry, Pondicherry University for their help in data measurement. The authors are thankful to CIF, Pondicherry University for instrumental facility.

References

[1] Kamat P. V. Photochemistry on Nonreactive and Reactive (Semiconductor) Surfaces. *Chem. Rev.*, **93**, P. 267–300 (1993).
[2] Guo H., Saalfrank P., Seideman T. Theory of Photoinduced Surface Reactions of Admolecules. *Prog. Surf. Sci.*, **62**, P. 239–303 (1999).
[3] Zimmermann F. M., Ho W. State Resolved Studies of Photochemical Dynamics at Surfaces. *Surf. Sci. Rep.*, **22**, P. 127–247 (1995).
[4] Hagfeld A., Gratzel M. Molecular Photovoltaics. *Acct. Chem. Res.*, **33**, P. 269–277 (2000).
[5] Forrest S. R. The Limits to Organic Photovoltaic Cell Efficiency. *MRS Bull.*, **30**, P. 28–32 (2005).
[6] Galperin M., Nitzan A. Current-Induced Light Emission and Light-Induced Current in Molecular-Tunneling Junctions. *Phys. Rev. Lett.*, **95**, P. 206802-1–4 (2005).
[7] O'Regan B., Gratzel M. A Low-cost, High-efficiency Solar Cell based on Dye-sensitized Colloidal TiO_2 films. *Nature*, **353**, P. 737–740 (1991).
[8] O'Regan B., Gratzel M. Photoelectrochemical Cells. *Nature*, **414**, P. 338–344 (2001).
[9] Yang L., Jiang X., Yang M. Improvement of Surface-enhanced Raman Scattering Performance for Broad Band Gap Semiconductor Nanomaterial (TiO_2): Strategy of Metal Doping. *Appl. Phys. Lett.*, **99**, P. 111114-1–3 (2011).
[10] Kalayanasundaram K., Gratzel M. Applications of Functionalized Transition Metal Complexes in Photonic and Optoelectronic Devices. *Coord. Chem. Rev.*, **77**, P. 347– 414 (1998).
[11] Boroda Y. G., Calhoun A., Voth G. A. A Theory for Electron Transfer Across the Electrode/electrolyte Interface Involving more than one Redox Ion. *J. Chem. Phys.*, **107**, P. 8940–8954 (1997).
[12] Cong Y., Tian B. Z., Zhang J. L. Improving the Thermal Stability and Photocatalytic Activity of Nanosized Titanium Dioxide via La^{3+} and N co-doping. *Appl. Catal. B*, **101**, P. 376–381 (2011).
[13] Rengifo-Herrera J. A., Pierzchaa K., Sienkiewicz A., Forr L., Kiwi J., Moser J. E., Pulgarin C. Synthesis, Characterization, and Photocatalytic Activities of Nanoparticulate N, S-codoped TiO_2 having Different Surface-to-volume Ratios. *J. Phys. Chem. C*, **114**, P. 2717–2723 (2010).
[14] Liu S., Xie T. H., Chen Z., Wu J. T. Highly active V-TiO_2 for Photocatalytic Degradation of Methyl Orange. *Appl. Surf. Sci.*, **255**, P. 8587–8592 (2009).
[15] Yang Q. J., Choi H., Chen Y. J., Dionysiou D. D. Heterogeneous Activation of Peroxymonosulfate by Supported Cobalt Catalysts for the Degradation of 2,4- dichlorophenol in water: The Effect of Support, Cobalt Precursor, and UV Radiation. *Appl. Catal. B*, **77**, P. 300–307 (2008).
[16] Liu Y., Wei J. H., Xiong R., Pan C. X., Shi J. Enhanced visible light photocatalytic properties of Fe-doped TiO_2 nanorod clusters and monodispersed nanoparticles. *Appl. Surf. Sci.*, **257**, P. 8121–8126 (2011).

[17] Han C., Pelaez M., Likodimos V., Kontos A.G., Falaras P., O'Shea K., Dionysiou D.D. Size-Tunable Hydrothermal Synthesis of SnS(2) Nanocrystals with High Performance in Visible Light-Driven Photocatalytic Reduction of Aqueous Cr(VI). *Appl. Catal. B*, **107**, P. 77–87 (2011).
[18] Asahi R., Morikawa T., Ohwaki T., Aoki K., Taga Y. Visible-Light Photocatalysis in Nitrogen-Doped Titanium Oxides. Science, P. 269–271 (2001).
[19] Sekiya T., Kamei S., Kurita S. Luminescence of Anatase TiO_2 Single Crystals Annealed in Oxygen Atmosphere. *J. Luminescence*, **1140**, P. 87–89 (2000).
[20] Rodríguez R., Jiménez-Sandoval S., Estevez M., Vargas S. Defec-Induced Luminescence in Co(II)-doped Anatase TiO_2 Prepared by the Sol-Gel Method. *J. Non-Crystalline Solids*, **351**, P. 167–172 (2005).
[21] Anbalagan K., Ganeshraja A. S., Maharaja Mahalakshmi C. Excited Nanoscale-TiO_2 Induced Interfacial Electron Transfer Reaction of Redox Active Cobalt(III)-alkyl Amine Complex and the Solid Surface. *Met. Chem. Phys.*, **134**, P. 747–754 (2012).
[22] Anbalagan K. UV-Sensitized Generation of Phasepure Cobalt-Doped Anatase: $Co_xTi_{1-x}O_{2-\delta}$ Nanocrystals with Ferromagnetic Behavior Using Nano-TiO_2/cis- $[Co^{III}(en)_2(MeNH_2)Cl]^{2+}$. *J. Phys. Chem. C*, **115**, P. 3821–3832 (2011).
[23] Kelly C. A., Meyer G. J. Excited State Processes at Sensitized Semiconductor- Interfaces Characterized by Nanosecond Absorption Spectroscopy. *Coord. Chem. Rev.*, **211**, P. 295–315 (2001).
[24] Anbalagan K., Maharaja Mahalakshmi C., Ganeshraja A. S. Synthesis and Spectroscopic Characterization of Cobalt(III)-Alkyl Amine Complexes Showing Surface Affinity: Single Crystal X-ray Structure Determinations. *J. Mol. Struct.*, **1005**, P. 45–52 (2011).
[25] Kitson R. E. Simultaneous Spectrophotometric Determination of Cobalt, Copper and Iron. *Anal. Chem.*, **22**, P. 664–667 (1950).
[26] Suryanarayana C. Nanocrystalline Materials. *Inter. Mater. Rev.*, **40**, P. 41-64 (1995).
[27] Moazzami K., Murphy T. E., Phillips J. D., Cheung M. C-K., Cartwright A. N. Sub- Bandgap Photoconductivity in ZnO Epilayers and Extraction of Trap Density Spectra. *Semicond. Sci. Technol.*, **21**, P. 717–723 (2006).
[28] Comedi D., Heluani S. P., Villafuerte M., Arce R. D., Koropecki R. R. Power-law Photoconductivity Time Decay in Nanocrystalline TiO_2 Thin Films. *J. Phys.: Condens. Matter*, **19**, P. 486205 (10pp) (2007).
[29] Shimakawa K., Murata K., Matsunomo S., Naito H. Photo-Carrier Transport in Disordered Organic TPD Films. *J. Non-Cryst. Solids*, **352**, P. 1671–1674 (2006).
[30] Anbalagana K., Lydia I. S. Solvent Control on the Electron Transfer Reaction between $Co^{III}(en)_2Br(L)^{2+}$–$Fe(CN)_6^{-4}$ (L = aryl amines) by Regression Relationships: the PXRD and Electrochemical Investigations. *J. Phys. Org. Chem.*, **24**, P. 45–53 (2011).
[31] Xie Z., Burkalov V. M., Henry B. M., Kirov K. R., Smith H. E., Grovenor C. R. M., Assender H. E., Briggs G. A. D., Kano M., Tsukahara Y. Intensity-Dependent Relaxation of Photoconductivity in Nanocrystalline Titania Thin Films. *Phys. Rev. B*, **73**, P. 113317 (2006).
[32] Mele G., Ciccarella G., Vasapollo G., Garcia-Lopez E., Palmisano L., Schiavello M. Photocatalytic Degradation of 4-nitrophenol in Aqueous Suspension by using Polycrystalline TiO_2 Samples Impregnated with Cu(II)-phthalocyanine. *Appl. Catal. B*, **38**, P. 309–311 (2002).
[33] Anbalagana K., Lydia I. S. Homogeneous Solvation Controlled Photoreduction of Cobalt(III) Complexes in Aqueous 2-methyl-2-propanol Solutions Linear Solvation Energy Relationship and Cyclic Voltammetric Analyses. *Spectrochim. Acta A*, **69**, P. 964–970 (2008).
[34] Matsuo S., Sakaguchi N., Yamada K., Matsuo T., Wakita H. Role in Photocatalysis and Coordination Structure of Metal Ions Adsorbed on Titanium Dioxide Particles: A Comparison between Lanthanide and Iron Ions. *Appl. Surf. Sci.*, **228**, P. 233–244 (2004).
[35] Ardo S., Meyer G. J. Direct observation of Photodriven Intermolecular Hole Transfer Across TiO_2 Nanocrystallites: Lateral Self-exchange Reactions and Catalyst Oxidation. *J. Am. Chem. Soc.* **132**, P. 9283–9285 (2010).
[36] Creutz C., Brunschwig B. S., Sutin N. Interfacial Charge Transfer Absorption: 3. Application to Semiconductor-Molecule Assemblies. *J. Phys. Chem. B*, **110**, P. 25181–25190 (2006).
[37] Ardo S., Sun Y., Staniszewski A., Castellano F. N., Meyer G. J. Stark-like Effects after Excited State Interfacial Electron Transfer at Sensitized TiO_2 Nanocrystallites. *J. Am. Chem. Soc.*, **132**, P. 6696–6709 (2010).

[38] Minero C., Mariella G., Maurino V., Pellizzetti E. Photocatalytic Transformation of Organic Compounds in the Presence of Inorganic Anions. 1. Hydroxyl-Mediated and Direct Electron-Transfer Reactions of Phenol on a Titanium Dioxide Fluoride System. Langmuir, **16**, P. 2632–2641 (2000).

[39] Ohko Y., Hashimoto K., Fujishima A. Kinetics of Photocatalytic Reactions under Extremely Low-Intensity UV Illumination on Titanium Dioxide Thin Films. *J. Phys. Chem. A*, **101**, P. 8057–8062 (1997).

[40] Wu J. C. S., Chen C. H. A Visible-Light Response Vanadium-Doped Titania Nanocatalyst by Sol–Gel Method. *J. Photochem. Photobiol. A*, **163**, P. 509–515 (2004).

[41] Hamadanian M., Reisi-Vanani A., Majedi A. Sol–Gel Preparation and Characterization of Co/TiO_2 Nanoparticles: Application to the Degradation of Methyl Orange. *J. Iran. Chem. Soc.*, **7**, P. S52–S58 (2010).

[42] Anbalagan K., Stephen L. D. UV-Sensitized Nanomaterial Semiconductor Catalytic Reduction of $Co^{III}(N–N)_3^{3+}$/nm-TiO_2 and Co:TiO_2 Formation: SEM-EDX and HRTEM Analyses. *Transition Met. Chem.*, **34**, P. 915–923 (2009).

[43] Baiju K.V., Shajesh P., Wunderlich W., Mukundan P., Kumar S. R., Warrier K. G. K., Effect of Tantalum Addition on Anatase Phase Stability and Photoactivity of Aqueous Sol–Gel Derived Mesoporous Titania. *J. Mol. Catal. A*, **276**, P. 41–46 (2007).

[44] Srivatsa K. M. K., Chhikara D., Senthil Kumar M. Synthesis of Anatase Titania Nanostructures at Room Temperature by PECVD Technique. *J. Mater. Sci. Technol.*, **27**, P. 696–700 (2011).

[45] Santhosh, S. M., Swetha S., Geetha, S., Balakrishna R. Erratum to "Structure and Photocatalytic Activity of $Ti_{1-X}M_xO_2$(M = Zr, Co and Mo) Synthesized by Pulverized Solid State Technique". *Cent. Eur. J. Chem.*, **8**, P. 453–460 (2010).